OPEN ACCESS
IOP Publishing
Journal of Physics G: Nuclear and Particle Physics
J. Phys. G: Nucl. Part. Phys. **48** (2021) 085102 (28pp)
https://doi.org/10.1088/1361-6471/abcdf6

Extended analytical solutions of the Bohr Hamiltonian with the sextic oscillator

G Lévai[1,*] **and J M Arias**[2,3]

[1] Institute for Nuclear Research (Atomki), P. O. Box 51, H-4001 Debrecen, Hungary
[2] Departamento de Física Atómica, Molecular y Nuclear. Facultad de Física, Universidad de Sevilla, Apartado 1065, 41080 Sevilla, Spain
[3] Instituto Carlos I de Física Teórica y Computacional, Universidad de Granada, Fuentenueva s/n, 18071 Granada, Spain

E-mail: levai@atomki.hu and ariasc@us.es

Received 22 July 2020, revised 15 September 2020
Accepted for publication 25 November 2020
Published 8 July 2021

Abstract

Low-lying collective quadrupole states in even–even nuclei are studied for the particular case of a γ-unstable potential within the Bohr Hamiltonian. In particular, the quasi-exactly solvable β-sextic potential is extended to cover the most relevant part of the low-lying spectra in nuclei. In previous papers (2004 *Phys. Rev. C* **69** 014304, 2010 *Phys Rev. C* **81** 044304), the same situation was solved for β-wavefunctions with up to one node ($M = 0, 1$), which are relevant for the first few low-lying states. Here, the model space is enlarged by including β-wavefunctions also with two nodes ($M = 2$), which generate many more states, in order to make it useful for actual fittings and more detailed checking of shape phase transitions between spherical and γ-unstable β-deformed shapes in nuclei. In addition to the energy eigenvalues and wavefunctions, closed analytical formulas are obtained for electric quadrupole and monopole transition probabilities too. The model is applied to the chains of even Ru and Pd isotopes to illustrate the transition between the spherical and deformed γ-unstable phases. These applications indicate that the optional extension of the model with a phenomenologic rotational term $L \cdot L$ is consistent with the experimental data.

Keywords: shape phase transitions in nuclei, gamma-unstable nuclei, quasi-exactly solvable potentials

(Some figures may appear in colour only in the online journal)

*Author to whom any correspondence should be addressed.

1. Introduction

The description of the low-lying collective quadrupole states in nuclei is a major topic in nuclear physics. An important advance was the introduction of the Bohr Hamiltonian (BM) for describing quadrupole oscillations of the nuclear surface in terms of two shape variables and the Euler angles [1]. The intrinsic variables are usually called β, that measures the deviation from sphericity, and γ, that measures the deviation from axial symmetry.

Later on, in the 70's, the interacting Boson model (IBM) was introduced to study the same system but exploiting the symmetries of the problem [2]. Although this model is formulated from the beginning in second quantization form, one can also introduce intrinsic shape parameters equivalent to β and γ for shape characterization. For this purpose, typically, a variational formulation in terms of intrinsic states has been used [3, 4].

In 2000, Iachello proposed a description of nuclear shape phase transitions and critical points based on the BM Hamiltonian [5]. In this first such model the transition from spherical to γ-unstable nuclear shapes was approximated by an infinite square well potential in the β variable. This situation was associated with the so called $E(5)$ critical point symmetry. Since then, many studies on shape phase transitions and various critical point symmetries have been done within both BM and IBM [6–11].

In connection to the BM model, depending on the selection of the interaction potential $V(\beta, \gamma)$ the solving of the corresponding Schrödinger equation is analytically feasible or not. Numerical solution of the Bohr Hamiltionian can be obtained (see e.g. references [12, 13]), however exactly solvable models also have the advantage that the transitions through critical points and the symmetries associated with them can be described analytically in a fully controllable way. Obviously, the range of exactly solvable Bohr Hamiltonians is limited. However, there are several selections that, although not exactly solvable, allow to get exact solutions for parts of the eigenvalues and eigenfunctions of the Bohr Hamiltionian. These potentials are called quasi-exactly solvable (QES) [14, 15]. One of these is the case of a γ-independent potential with a sextic β dependence. Depending on the parameters, this potential has a flexible tunable shape with a spherical and/or a deformed minimum, so it is suitable to investigate transition between various shape phases. In references [16, 17] this situation was solved for a restricted set of states with polynomial solutions in β^2 up to the order $M = 1$ that included only up to seniority $\tau = 3$ and angular momentum $L = 6$. This was important, since it provided tools to study and characterise shape phase transitions between spherical and β-deformed shapes. However, an extension of the model space is clearly needed for deeper tests including spectra, transition rates and analysis of the shape phase transitions with more observables.

In this manuscript the QES γ-unstable plus sextic β-potential is worked out for solutions containing polynomials in β^2 up to the order $M = 2$. This provides exact solutions for many more low-lying states with seniority up to $\tau = 5$ and angular momenta up to $L = 10$. Similarly to the original, restricted version of the model, the extended formalism seems applicable to further types of potentials used in the BM Hamiltonian: γ-stable triaxial [18], γ-stable prolate [19], γ-rigid triaxial [20] and γ-rigid prolate [21] nuclei (see reference [22] for a review). The sextic potential was also applied in a numerical study to describe double-well structures [23]. Finally, it is worth mentioning that in a recent work, reference [24], a numerical study including higher QES levels was presented. There a new integer parameter, k, was introduced. Our analytical study would correspond to $k = 2$ that, as stated by the authors, seems to be in many cases the best approximation for phase transition studies.

The manuscript is structured as follows. In section 2, the sextic oscillator is revisited and solutions are worked out for $M = 2, 1, 0$. The structure of the spectrum, its evolution in terms of the model parameters, and the form of the wavefunctions are presented. In addition, the

formalism to get analytically the relevant electromagnetic transition rates is given in section 2 and in the appendix. Section 3 is devoted to the application of the model to the chains of Ru and Pd isotopes. Finally, section 4 is for summarising the main results of this work.

2. The sextic oscillator

The Bohr Hamiltonian describes the quadrupole oscillations of the nucleus in terms of the intrinsic β and γ shape variables as [1]

$$H = -\frac{\hbar^2}{2B}\left(\frac{1}{\beta^4}\frac{\partial}{\partial\beta}\beta^4\frac{\partial}{\partial\beta} + \frac{1}{\beta^2\,\sin\,3\gamma}\frac{\partial}{\partial\gamma}\,\sin\,3\gamma\frac{\partial}{\partial\gamma}\right.$$
$$\left. - \frac{1}{4\beta^2}\sum_k \frac{\hat{Q}_k^2}{\sin^2\left(\gamma - \frac{2}{3}\pi k\right)}\right) + V(\beta,\gamma)\ , \tag{1}$$

where B is a mass parameter and $\hat{Q}_k$ are the angular momentum projections on the intrinsic axes. In general, $V(\beta,\gamma)$ is a function of both intrinsic variables. A simplified version of this equation is obtained if the potential is independent of the γ variable, $V(\beta,\gamma) = U(\beta)$. This situation corresponds to the so-called γ-unstable nuclei, and in this case the β-dependence can be separated into an equation reminescent of the radial Schrödinger equation by substituting

$$\Psi(\beta,\gamma,\theta_i) = \beta^{-2}\,\phi(\beta)\Phi(\gamma,\theta_i) \tag{2}$$

in equation (1):

$$-\frac{\mathrm{d}^2\phi}{\mathrm{d}\beta^2} + \left(\frac{(\tau+1)(\tau+2)}{\beta^2} + u(\beta)\right)\phi = \epsilon\phi\ , \tag{3}$$

where $\epsilon = \frac{2B}{\hbar^2}E$ and $u(\beta) = \frac{2B}{\hbar^2}U(\beta)$. In (3), τ originates from the angular equation, in analogy with the reduction of the three-dimensional Schrödinger equation with a spherically symmetric potential to the radial Schrödinger equation.

The $u(\beta)$ potential was chosen previously [16, 17] as the sextic oscillator, which belongs to the family of QES potentials [15]. In this case its coupling coefficients are correlated and are expressed in terms of two parameters, a and b and a fixed constant, c^π as follows:

$$u(\beta) = (b^2 - 4ac^\pi)\beta^2 + 2ab\beta^4 + a^2\beta^6 + u_0^\pi\ . \tag{4}$$

It can be noted that the problem can be reparametrized by using a scale factor $\beta = a^{-1/4}x$ (see e.g. reference [22]), in which case the energy is also rescaled as $\epsilon(a,b) = a^{1/2}\epsilon(1,a^{-1/2}b)$. This transformation seemingly reduces the number of parameters, however, it also affects the B parameter. In practice one can chose either $a^{-1/2}b$ and B as parameters, or can fix B to a constant and use a and b. In what follows, the latter option will be used, furthermore, for convenience, we shall use E for the reduced energy instead of ϵ.

The solutions of equation (3) with the potential (4) are written as

$$\phi(\beta) \sim \beta^{\tau+2}\,\exp\left(-\frac{a}{4}\beta^4 - \frac{b}{2}\beta^2\right)P^{(M)}(\beta^2)\ , \tag{5}$$

where $P^{(M)}(\beta^2)$ is an M'th order polynomial in β^2. It is seen that the physical dimension of a and b is [length]$^{-4}$ and [length]$^{-2}$, respectively. With this functional form, the coefficients

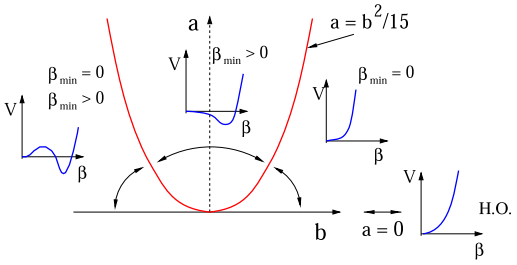

Figure 1. Different possible shapes for the energy surface $u(\beta)$ in the parameter (a, b) model space for $M = 2$, corresponding to $c^+ = 15/4$ and $c^- = 17/4$. The parabola $a = b^2/15$ separates spherical from deformed shapes for $b \geqslant 0$ and the deformed shapes from the region in which one spherical and one deformed minima coexist ($b \leqslant 0$).

of the polynomial can be determined after finding the roots of an $(M + 1)$'th order algebraic equation. In references [16, 17] the $M = 0$ and $M = 1$ cases were considered. It was also found that the coefficient of the quadratic term depends on $\tau + 2M$ combination. Thus, in order to have the same potential for different values of M, one has to introduce the constant

$$2c^\pi = \tau + 2M + \frac{7}{2}. \tag{6}$$

Note that this constant will be slightly different for even and odd values of τ, hence the superscript π. In references [16, 17], $c^+ = 11/4$ and $c^- = 13/4$ were considered, corresponding to $\tau + 2M = 2$ and 3, for even and odd values of τ, respectively. Here we extend the method to $M = 2$, in which case a cubic algebraic equation has to be solved. Now we have to take $c^+ = 15/4$ and $c^- = 17/4$ corresponding to $\tau + 2M = 4$ and 5, respectively.

Before deriving the solutions, let us first examine the possible shapes of the potential (4). The sign of the coupling coefficients $b^2 - 4ac^\pi$, $2ab$ and a^2 are crucial in this analysis. One finds that a^2 is always non-negative, while the sign of $2ab$ depends on the sign of b, because the normalizability of the wavefunction (5) prescribes $a \geqslant 0$. The coefficient $b^2 - 4ac^\pi$ can be positive, negative or zero. When neither $b^2 - 4ac^\pi$ or $2ab$ is negative, then $u(\beta)$ increases monotonously, so the energy surface has a single minimum at $\beta = 0$. If $b^2 - 4ac^\pi < 0$, then $u(\beta)$ has a maximum at $\beta = 0$ and a minimum at $\beta > 0$, irrespective of the sign of $2ab$, i.e. of b. The most complex shape occurs when $b^2 - 4ac^\pi > 0$ and $b < 0$ holds: in this case there are two minima, one at $\beta = 0$ and another one at $\beta > 0$, and there is a maximum in between. It can be shown that the deformed minimum is always deeper than the spherical one. These domains are separated in the (a, b) parameter space by the critical parabola defined by $b^2 - 4ac^\pi = 0$. As it was discussed above, the potential, as well as the critical parabola is slightly different for states with even and odd values of τ. In figure 1 we present a scheme of the possible energy surfaces in the model space (adapted from reference [17] to the extended model).

A more quantitative analysis can be performed by examining the location of the extrema, determined by the relation

$$(\beta_0^\pi)^2 = \frac{1}{3a}[-2b \pm (b^2 + 12ac^\pi)^{1/2}] \ . \tag{7}$$

Whenever the right handside of (7) is positive, the '+' sign determines the non-zero minimum, while the '−' sign sets the maximum for $b < 0$.

This slight difference in τ-parity, which resembles the parity-dependence of radial potentials in three spatial dimensions, manifests itself near $\beta = 0$ in the coefficient of the β^2 term. In references [16, 17] this slight ambiguity was handled by selecting the constant terms u_0^+ and u_0^- such that the minima of the two potentials are set at the same energy. This requirement can be fulfiled by setting $u_0^+ = 0$ and

$$u_0^- = \begin{cases} (b^2 - 15a)(\beta_0^+)^2 - (b^2 - 17a)(\beta_0^-)^2 & \\ +2ab[(\beta_0^+)^4 - (\beta_0^-)^4] + a^2[(\beta_0^+)^6 - (\beta_0^-)^6] & \text{if } b < (15a)^{1/2} \\ -(b^2 - 17a)(\beta_0^-)^2 - 2ab(\beta_0^-)^4 - a^2(\beta_0^-)^6 & \text{if } (15a)^{1/2} < b < (17a)^{1/2} \\ 0 & \text{if } b > (17a)^{1/2}, \end{cases} \tag{8}$$

where $\beta_0^\pm$ is the location of the non-zero minimum of $u^\pm(\beta)$ discussed above.

For $M = 2$ the normalised solutions of equation (5) are written as

$$\phi_\alpha(\beta) = N_\alpha \beta^{\tau+2}(1 + d_\alpha\beta^2 + g_\alpha\beta^4) \exp\left(-\frac{a}{4}\beta^4 - \frac{b}{2}\beta^2\right) , \tag{9}$$

where α stands for the quantum numbers (ξ, τ). Here $\xi = 1$, 2 and 3 is a traditional notation and is related to the n node number of the β-wavefunction as $\xi = n + 1$. Note that equation (9) is also valid for $M < 2$: in these cases one has to select $d_\alpha = g_\alpha = 0$ for $M = 0$ or $g_\alpha = 0$ for $M = 1$.

According to the formalism of the sextic oscillator as presented in reference [15] (see equation (2.2.6) and (2.2.7) there), the polynomial part of the wavefunction satisfies the following equations:

$$P^{(M)}(\beta^2) = \sum_{i=0}^{M} C_{Mi}\beta^{2i} , \tag{10}$$

$$\hat{X}P(\beta^2) = EP(\beta^2) \tag{11}$$

and

$$\hat{X} \equiv -\left(\frac{\mathrm{d}^2}{\mathrm{d}\beta^2} + \frac{4s-1}{\beta}\frac{\mathrm{d}}{\mathrm{d}\beta}\right) + 2b\left(\beta\frac{\mathrm{d}}{\mathrm{d}\beta} + 2s\right) + 2a\beta^2\left(\beta\frac{\mathrm{d}}{\mathrm{d}\beta} - 2M\right), \tag{12}$$

where

$$s = \frac{\tau}{2} + \frac{5}{4}, \tag{13}$$

i.e. $2s = \tau + 5/2$ and $4s - 1 = 2\tau + 4$.

Let us now consider the cases $M = 0$, $M = 1$ and $M = 2$ and substitute (10) and (12) into (11). Let's keep $\tau + 2M = 4$ for even values of τ and $\tau + 2M = 5$ for odd values of τ. In the following we will use the notation

$$\lambda^{(M)} = E^{(M)} - 4bs. \tag{14}$$

For $M = 0$ (i.e. $\tau = 4$ and 5), one has $P^{(0)}(\beta^2) = C_{00}$ and

$$C_{00}\left(-\lambda^{(0)}\right) = 0 , \tag{15}$$

i.e.

$$E^{(0)} = 4bs. \tag{16}$$

Taking $\tau = 4$ and $\tau = 5$ one gets

$$E^{(0)}_{\xi\tau} = E^{(0)}_{14} = 13b \tag{17}$$

and

$$E^{(0)}_{\xi\tau} = E^{(0)}_{15} = 15b. \tag{18}$$

For $M = 1$ (i.e. $\tau = 2$ and 3), the polynomial is

$$P^{(1)}(\beta^2) = C_{10} + C_{11}\beta^2, \tag{19}$$

and equation (11) reduces to

$$0 = -C_{10}\lambda^{(1)} - 8sC_{11} + \beta^2[-4aC_{10} + C_{11}(4b - \lambda^{(1)})]. \tag{20}$$

This leads to the algebraic equation

$$0 = \begin{pmatrix} -\lambda^{(1)} & -8s \\ -4a & 4b - \lambda^{(1)} \end{pmatrix} \begin{pmatrix} C_{10} \\ C_{11} \end{pmatrix}. \tag{21}$$

Taking the determinant as 0, the solutions are given as

$$\lambda^{(1)}_{\pm} = 2b \pm 2\left(b^2 + 8as\right)^{1/2}, \tag{22}$$

$$E^{(1)}_{\pm} = 4bs + \lambda^{(1)}_{\pm}. \tag{23}$$

After substituting these values into (21) and determining the C_{1i} coefficients, it turns out that (19) is nodeless for the lower sign $(-)$ and has one node for the upper sign $(+)$. Taking now $\tau = 2$ and 3, we have $s = 9/4$ and $11/4$ in the two cases, respectively. The energy eigenvalues and the coefficients of the polynomial part of the wavefunction are displayed in table 1.

In the $M = 2$ (i.e. $\tau = 0$ and 1) case the polynomial is

$$P^{(2)}(\beta^2) = C_{20} + C_{21}\beta^2 + C_{22}\beta^4\ , \tag{24}$$

leading to

$$\begin{aligned} 0 = &-C_{20}\lambda^{(2)} - 8sC_{21} + \beta^2[-8aC_{20} + C_{21}(4b - \lambda^{(2)}) - 8(2s+1)C_{22}] \\ &+ \beta^4[-4aC_{21} + (8b - \lambda^{(2)})C_{22}]. \end{aligned} \tag{25}$$

This leads to the algebraic equation

$$0 = \begin{pmatrix} -\lambda^{(2)} & -8s & 0 \\ -8a & 4b - \lambda^{(2)} & -8(2s+1) \\ 0 & -4a & 8b - \lambda^{(2)} \end{pmatrix} \begin{pmatrix} C_{20} \\ C_{21} \\ C_{22} \end{pmatrix}. \tag{26}$$

Taking the determinant 0, a cubic algebraic equation is obtained for $\lambda^{(2)}$:

$$0 = (\lambda^{(2)})^3 - 12b(\lambda^{(2)})^2 - 32\left(a(4s+1) - b^2\right)\lambda^{(2)} + 512sab \tag{27}$$

Table 1. Explicit form of the lowest few energy eigenvalues and the coefficients appearing in the wavefunctions. The $\lambda_i^{(M)}$ and $\widetilde{\lambda}_i^{(M)}$ eigenvalues refer to τ-even and τ-odd states, corresponding to the choices $2M+\tau=4$ and 5, respectively. For the notation of the energy eigenvalues here $E_{\xi,\tau}$ was used, where the actual ξ and τ quantum numbers are displayed along with the relevant value of M.

ξ	τ	M	$E_{\xi,\tau}$	$d_{\xi,\tau}$	$g_{\xi,\tau}$
1	0	2	$5b+\begin{cases}\lambda_2^{(2)} & b>0\\ \lambda_1^{(2)} & b<0\end{cases}$	$\begin{cases}-\dfrac{\lambda_2^{(2)}}{10} & b>0\\ -\dfrac{\lambda_1^{(2)}}{10} & b<0\end{cases}$	$\begin{cases}-\dfrac{2a\lambda_2^{(2)}}{5(8b-\lambda_2^{(2)})} & b>0\\ -\dfrac{2a\lambda_1^{(2)}}{5(8b-\lambda_1^{(2)})} & b<0\end{cases}$
1	2	1	$9b+\lambda_-^{(1)}$	$-\frac{1}{18}\lambda_-^{(1)}$	0
1	4	0	$13b$	0	0
2	0	2	$5b+\lambda_3^{(2)}$	$\frac{1}{10}\lambda_3^{(2)}$	$-\frac{2a\lambda_3^{(2)}}{5(8b-\lambda_3^{(2)})}$
2	2	1	$9b+\lambda_+^{(1)}$	$-\frac{1}{18}\lambda_+^{(1)}$	0
3	0	2	$5b+\begin{cases}\lambda_1^{(2)} & b>0\\ \lambda_2^{(2)} & b<0\end{cases}$	$\begin{cases}-\dfrac{\lambda_1^{(2)}}{10} & b>0\\ -\dfrac{\lambda_2^{(2)}}{10} & b<0\end{cases}$	$\begin{cases}-\dfrac{2a\lambda_1^{(2)}}{5(8b-\lambda_1^{(2)})} & b>0\\ -\dfrac{2a\lambda_2^{(2)}}{5(8b-\lambda_2^{(2)})} & b<0\end{cases}$
1	1	2	$7b+\begin{cases}\widetilde{\lambda}_2^{(2)} & b>0\\ \widetilde{\lambda}_1^{(2)} & b<0\end{cases}$	$\begin{cases}-\dfrac{\widetilde{\lambda}_2^{(2)}}{14} & b>0\\ -\dfrac{\widetilde{\lambda}_1^{(2)}}{14} & b<0\end{cases}$	$\begin{cases}-\dfrac{2a\widetilde{\lambda}_2^{(2)}}{7(8b-\widetilde{\lambda}_2^{(2)})} & b>0\\ -\dfrac{2a\widetilde{\lambda}_1^{(2)}}{7(8b-\widetilde{\lambda}_1^{(2)})} & b<0\end{cases}$
1	3	1	$11b+\widetilde{\lambda}_-^{(1)}$	$-\frac{1}{22}\widetilde{\lambda}_-^{(1)}$	0
1	5	0	$15b$	0	0
2	1	2	$7b+\widetilde{\lambda}_3^{(2)}$	$\frac{1}{14}\lambda_3^{(2)}$	$-\frac{2a\widetilde{\lambda}_3^{(2)}}{7(8b-\widetilde{\lambda}_3^{(2)})}$
2	3	1	$11b+\widetilde{\lambda}_+^{(1)}$	$-\frac{1}{22}\widetilde{\lambda}_+^{(1)}$	0
3	1	2	$7b+\begin{cases}\widetilde{\lambda}_1^{(2)} & b>0\\ \widetilde{\lambda}_2^{(2)} & b<0\end{cases}$	$\begin{cases}-\dfrac{\widetilde{\lambda}_1^{(2)}}{14} & b>0\\ -\dfrac{\lambda_2^{(2)}}{14} & b<0\end{cases}$	$\begin{cases}-\dfrac{2a\widetilde{\lambda}_1^{(2)}}{7(8b-\widetilde{\lambda}_1^{(2)})} & b>0\\ -\dfrac{2a\widetilde{\lambda}_2^{(2)}}{7(8b-\widetilde{\lambda}_2^{(2)})} & b<0\end{cases}$

$$\equiv A(\lambda^{(2)})^3+B(\lambda^{(2)})^2+C\lambda^{(2)}+D. \tag{28}$$

Introducing the quantities

$$p=\frac{3AC-B^2}{9A^2}=-\frac{16}{3}[b^2+2a(4s+1)], \tag{29}$$

and

$$q=\frac{B^3}{27A^2}-\frac{BC}{6A^2}+\frac{D}{2A}=-64ab, \tag{30}$$

one finds that p is always negative, while the sign of q is the opposite of the sign of b ($a\geqslant 0$ is a requirement to get normalizable states). Another critical quantity is

$$\mathcal{D}=q^2+p^3=-\frac{2^{12}}{3^3}\left[b^6+6b^4a(4s+1)+3a^2b^2(8s+5)(8s-1)+8a^3(4s+1)^3\right]. \tag{31}$$

It can be shown that $\mathcal{D} < 0$ holds in general, as $s > 5/4$ is always valid, due to equation (13). Under these circumstances, $\mathcal{D} < 0$, $p < 0$, the cubic algebraic equation (28) always has three real roots, which can be written as follows:

$$\lambda_1^{(2)} = -\frac{B}{3A} - 2r\cos\left(\frac{\phi}{3}\right) = 4b - 2r\cos\left(\frac{\phi}{3}\right) , \tag{32}$$

$$\lambda_2^{(2)} = -\frac{B}{3A} + 2r\cos\left(\frac{\pi}{3} - \frac{\phi}{3}\right) = 4b + 2r\cos\left(\frac{\pi}{3} - \frac{\phi}{3}\right) , \tag{33}$$

$$\lambda_3^{(2)} = -\frac{B}{3A} + 2r\cos\left(\frac{\pi}{3} + \frac{\phi}{3}\right) = 4b + 2r\cos\left(\frac{\pi}{3} + \frac{\phi}{3}\right) , \tag{34}$$

where

$$\cos(\phi) = \frac{q}{r^3}, \tag{35}$$

and

$$r = \pm|p|^{1/2} = \pm\left[\frac{16}{3}(b^2 + 2a(4s+1))\right]^{1/2}, \tag{36}$$

where the sign of r has to be the same as the sign of q.

After substituting the $\lambda_1^{(2)}$ values into (26) and determining the C_{2i} coefficients, it turns out that the polynomial (24) originating from $\lambda_3^{(2)}$ always has one node, while the other two have zero or two nodes, depending on the sign of r, q and thus of b. The energy eigenvalues and the coefficients of the polynomial part of the wavefunction are displayed in table 1. The $M = 2$ solutions correspond to $\tau = 0$ and $\tau = 1$ for the cases $2M + \tau = 4$ and 5. Note that this difference reflects in the difference in s (which is 5/4 and 7/4 in the two cases), and thus also in p in (29), r in (36) and thus in ϕ via (35).

A special situation occurs for $b = 0$, when some terms of the cubic equation (28) will be missing. In particular, $B = D = 0$ leads to an equation that can be solved directly. One finds that in this case $q = 0$, $\phi = \pi/2$, $\lambda_1^{(2)} = -[32a(4s+1)]^{1/2}$, $\lambda_2^{(2)} = [32a(4s+1)]^{1/2}$ and $\lambda_3^{(2)} = 0$.

The energy eigenvalues are obtained as

$$E_i^{(2)} = 4bs + \lambda_i^{(2)}. \tag{37}$$

The $\tau = 4$ configuration includes states with $L^\pi = 2^+, 4^+, 5^+, 6^+$ and 8^+, while for $\tau = 5$ one has $L^\pi = 2^+, 4^+, 5^+, 6^+, 7^+, 8^+$ and 10^+. In figure 2 a scheme of the spectrum for $M = 2, 1, 0$ is shown. In the figure, the quantum numbers used are ξ that is related to the number of zeroes (n) of the β-wave function ($\xi = n + 1$, as discussed before), τ that is the O(5) quantum number and gives the number of particles not coupled by pairs to zero angular momentum (seniority), and L that is the angular momentum linked to O(3). In addition, there is a hidden quantum number in the reduction from O(5) to O(3) that we call Δ and gives the number of triplets coupled to zero angular momentum.

2.1. The energy spectrum

In the practical applications it is more suitable to use the excitation energies with respect to the ground state E_{10}. Furthermore, the constants u_0^π used in equation (8) also have to be taken into

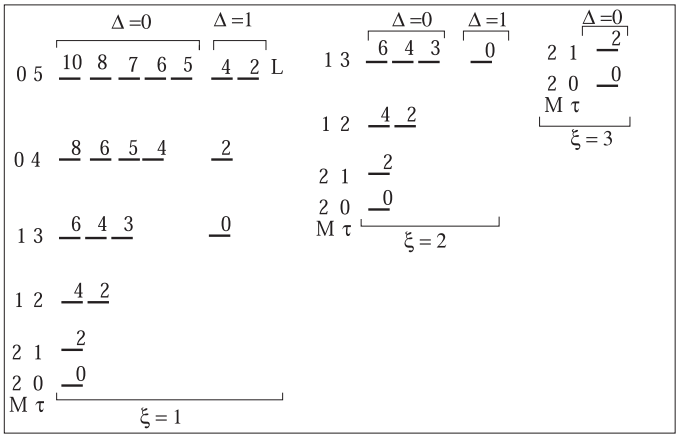

Figure 2. The schematic energy spectrum for the γ-unstable sextic oscillator with $M = 2, 1, 0$. The quantum labels are (ξ, τ, Δ, L).

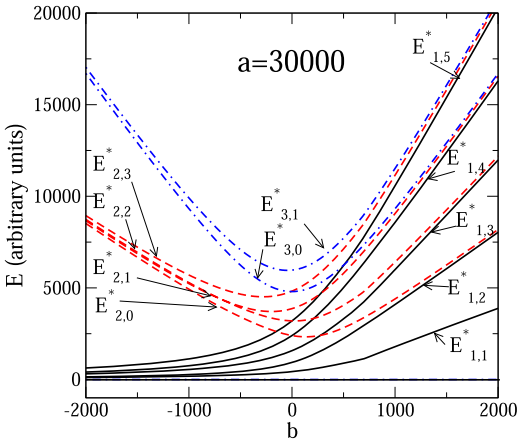

Figure 3. Energy spectrum as function of b, for fixed $a = 30\,000$.

account, so in what follows we shall use

$$E^*_{\xi\tau} = E_{\xi\tau} - E_{10} + u_0^\pi. \tag{38}$$

Figures 3 and 4 display the energy spectrum for a fixed value of a and b, respectively, while leaving the other parameter to vary in some domain. In the odd-τ curves there is a kink near $a = b^2/15$ and $a = b^2/17$, which is visible only for the low-lying levels. This is the consequence of matching the τ-even and τ-odd components of the energy spectrum by prescribing that the two slightly differing potentials (4) have their minima at the same energy. (See equation (8) for the details.)

It is seen in figure 3 that the energy levels tend to form groups for large $|b|$, and these group rearrange close to $b = 0$. For $b \to \infty$ the groups are characterized by a common value for $2\xi + \tau$, which is typical for the energy spectrum of the harmonic oscillator. Indeed, increasing

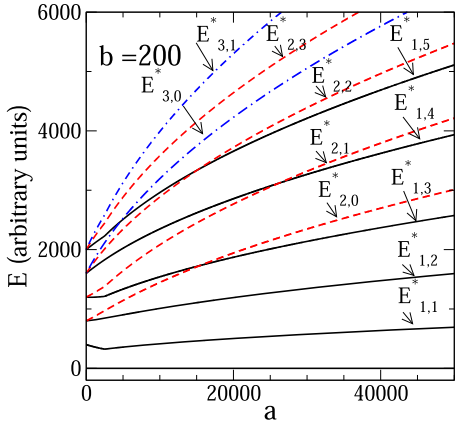

Figure 4. Energy spectrum as function of a, for fixed $b = 200$.

$b > 0$ and keeping a at constant value is basically equivalent with keeping b fixed and taking the $a = 0$ limit, which is nothing but the harmonic oscillator. For $b \to -\infty$ the groups contain the levels with the same ξ quantum number. It can be shown that the energy levels with $\xi = 1$, 2 and 3 tend asymptotically as 0, $-4b$ and $-8b$, respectively, as seen also in figure 3. This difference with respect to the $b \to \infty$ limit arises due to different behaviour of the $\lambda_i^{(2)}$ roots of the cubic algebraic equation (28) for $b > 0$ and $b < 0$, reflected also in table 1. The argument outlined for $b > 0$ does not hold here, because the $a \to 0$ limit would lead to unnormalizable wave functions (5).

The behaviour of the energy eigenvalues for fixed b and a varying is presented in figure 4 and is more regular: it shows a uniform increase of energy with increasing a. The relative position of the energy levels does not change too much, except for low values of a. For $a = 0$ the harmonic oscillator spectrum is recovered, together with the characteristic degeneracy pattern. In this case b corresponds to $\hbar\omega/2$.

Finally, in figure 5 the energy ratios that characterise the critical parabola in the (a, b) model space separating spherical from deformed shapes are given explicitly. It can be seen that our analytical results match perfectly with the numerical results for the critical point presented in reference [24] for some energy ratios (see the $k = 2$ case in table I of that reference).

2.2. The wavefunctions

The structure of the wavefunctions comes from the $U(5) \supset O(5) \supset O(3) \supset O(2)$ group chain associated with the problem which correspond to the eigenstates of the harmonic oscillator in five dimensions $(\beta, \gamma, \theta_i)$ (θ_i are the three Euler angles). These states are labelled by the quantum numbers $|N, \tau, \Delta, L, M\rangle$, where N is the number of phonons, τ, L and Δ are the seniority, the angular momentum and the auxiliary quantum number in the $O(5) \supset O(3)$ reduction, respectively discussed previously, while M is the projection of L on an axis in the lab frame. (Not to be confused with M in equation (5), where it denotes the degree of the polynomial part of the wavefunction.) The general form of the wavefunctions is:

$$\langle \beta, \gamma, \theta_i | \xi, \tau, \Delta, L, M\rangle = F_\xi^\tau(\beta) \sum_K \Phi_K^{\tau,\Delta,L}(\gamma) \mathcal{D}_{M,K}^{L*}(\theta_i), \tag{39}$$

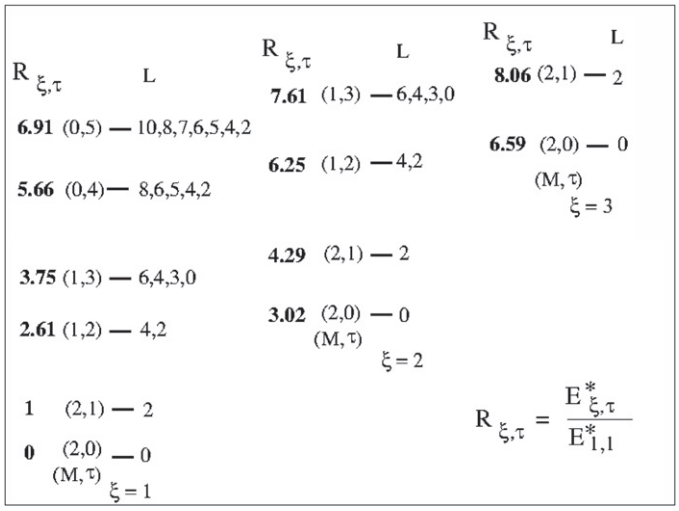

Figure 5. Characteristic energy ratios for the shape phase parabola separating the spherical and the deformed region in the model.

where the label ξ is related to N by $\xi = (N - \tau)/2 + 1$ and gives the number of zeroes of the radial wavefunction (excluding the ones at origin and at infinity) plus one. The sum is on the quantum number K that gives the projection of the angular momentum on the intrinsic symmetry axis (only can take even values for L even and odd values for L odd). In our case, the radial β-part is given by equation (9) where $\alpha = (\xi, \tau)$, $F^{\tau}_{\xi}(\beta) = \beta^{-2}\phi_{\xi,\tau}(\beta)$. The radial function we have determined with the polynomial parameters $d_{\xi,\tau}$ and $g_{\xi,\tau}$ given in table 1 is $\phi_{\xi,\tau}(\beta)$ (the square of the β^{-2} term cancels the β^4 part of the Jacobian). The Euler part $\mathcal{D}^{L*}_{M,K}(\theta_i)$ are the rotation D-matrices. Finally, the γ-functions have to be generated for the case of γ-independent vibrations. The computation of these wavefunctions was first done for a limited set of states ($L \leqslant 6$) by Bés [25]. Later on a more general treatment was done by Yannouleas and Pacheco [26]. More recently, Rowe, Turner and Repka presented an extensive work on the $\gamma-$wavefunctions [27] in which exact algebraic expressions of relevant matrix elements were obtained. We have followed the procedure given by Moshinsky [28] and used a Mathematica notebook code to generate the relevant wavefunctions up to $L = 10$. When possible, these results were checked against those given in reference [27]. Once the wavefunctions are constructed, transition probabilities are obtained by integrating the appropriate electromagnetic operator in all variables: β, γ and the three Euler angles θ_i.

Concerning the radial β-functions (9), as mentioned, they can be determined using the polynomial expressions calculated previously for the $M = 0$, 1 and 2 cases separately. These coefficients can be found in table 1. In addition, the normalization coefficients also have to be determined. These are calculated in the Appendix in terms of confluent hypergeometric functions. Figure 6 displays an example of the wavefunctions obtained for some values of the parameters a and b. These values are the ones obtained for a good description of ^{104}Ru that is close to the critical parabola but slightly deformed. In the left panel, the β-wave functions with $\xi = 1$ and different τ are displayed, neither of them have zeroes apart from those at the origin and at infinity (remember that $\xi = n + 1$). In the central panel the functions with $\xi = 2$ are presented for the different τ, all of them have one zero. In the right panel, the β-wavefunctions with $\xi = 3$ are plotted, all of them have two zeroes. In order to complete the image given in figure 6,

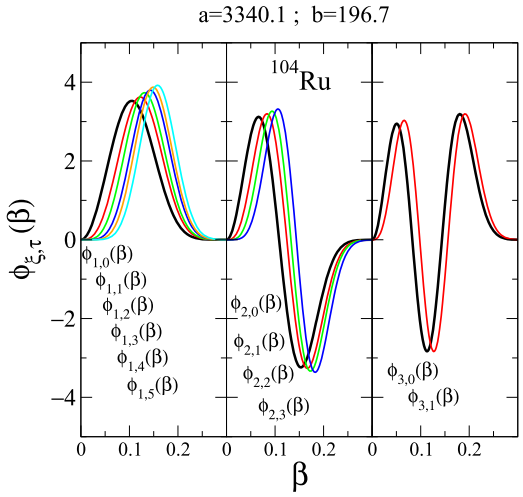

Figure 6. The β-wavefunctions $\phi_{\xi,\tau}(\beta)$ displayed for $a = 3340.1$ and $b = 196.7$ (corresponding to the fitted values for ^{104}Ru).

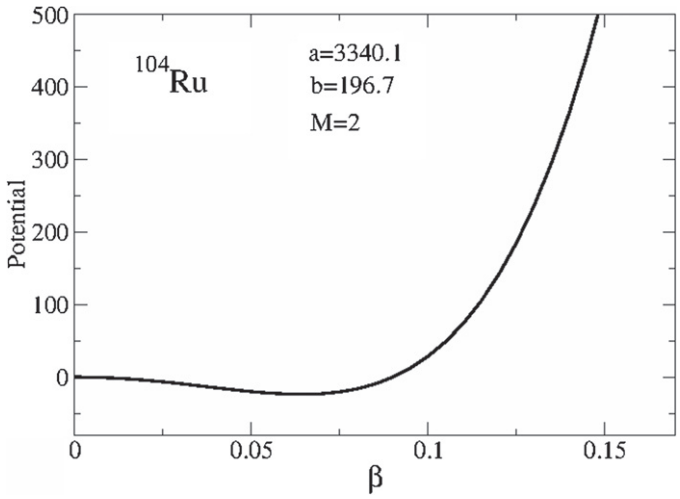

Figure 7. The β-potential for the case $a = 3340.1$ and $b = 196.7$ (corresponding to the fitted values for ^{104}Ru).

we present in figure 7 the potential corresponding to the case $a = 3340.1$ and $b = 196.7$ that are the values for which the β-wavefunctions are plotted in figure 6. The length is measured in units of 14.4 fm, which arises naturally if the energy, [energy $\times$ time] and mass are measured in units of keV, $\hbar$ and $2B$, respectively, where B is the mass of the given nucleus.

2.3. Electromagnetic transitions

Once the wavefunctions are known, transition probabilities are obtained by integrating the appropriate electromagnetic operator in all variables: β, γ and the three Euler angles θ_i. It

should be noted that the Jacobian in the (β, γ) intrinsic variables is $\beta^4|\sin 3\gamma|$. In the β integration, the part coming from the Jacobian cancels with our definition of the β-wavefunction in equation (2), that is with the β^{-4} coming from the square of $\beta^{-2}\phi(\beta)$.

The radial β integrals necessary to evaluate electromagnetic transition rates can also be calculated analytically using the explicit form of the wave functions and the appropriate transition operators.

2.3.1. E2 operator. Using the first-order electric quadrupole transition operator [5, 29]

$$T^{(\mathrm{E2})} = t\beta\left[D^{(2)}_{\mu,0}\cos\gamma + \frac{1}{\sqrt{2}}\left(D^{(2)}_{\mu,2} + D^{(2)}_{\mu,-2}\right)\sin\gamma\right] . \tag{40}$$

the relevant β matrix elements are

$$M(\mathrm{E2};\alpha\to\gamma) = W^1_{\alpha,\gamma}, \tag{41}$$

where the general form of $W^{\delta}_{\alpha,\gamma}$ is presented in the appendix.

It is sufficient to calculate the integrals with $\Delta\tau = \pm 1$, because the remaining matrix elements will be zero due to the τ-dependent components of the total wavefunctions. It should be noted that in order to get the corresponding transition probabilities the above radial integrals should be evaluated as well as those in the γ and Euler angle parts. The B(E2) values are defined as,

$$\begin{aligned} &B(\mathrm{E2};\xi',\tau',\Delta',L',M'\to\xi,\tau,\Delta,L,M) \\ &\quad = \frac{1}{\sqrt{2L'+1}}\left|\langle\xi,\tau,\Delta,L\|T^{(\mathrm{E2})}\|\xi',\tau',\Delta',L'\rangle\right|^2, \end{aligned} \tag{42}$$

where the double bar indicates reduced matrix element.

A sample of B(E2) values is displayed in figure 8 for parameter values corresponding to the critical parabola. It is notable that they are fixed along the parabola, so they supply benchmark numbers for the transition between various shape phases. A complete account of all B(E2) values for the parabola transition line and $M = 2, 1, 0$ is given in tables 2 and 3. Again, the present analytical results match perfectly with the numerical results for the critical point presented in reference [24] for some B(E2) ratios (see the $k = 2$ case in table I of that reference).

It seems that the deexcitation properties of the $L^\pi = 0^+$ states are important to identify them properly. In figure 9 the B(E2) values for $L^\pi = 0^+$ states at the critical parabola are given as a reference.

2.3.2. E0 transitions. For the electric monopole transitions the $\delta = 2$ case of (A.3) has to be considered since the monopole transition operator is proportional to β^2,

$$T^{(\mathrm{E0})} = q\beta^2. \tag{43}$$

The analytical results for the $T^{(\mathrm{E0})}\beta$-matrix elements are given explicitly in equation (A.6). With this expression the evolution of the E0 transition involving the three lowest 0^+ states can be studied as the function of the model parameters. Transitions from the $(\xi,\tau) = (1,3)$ and $(2,3)0^+$ levels to the ground state with $(1,0)0^+$ are expected to be forbidden due to the selection rules on τ, while transitions from the $(2,0)0^+$ and $(3,0)0^+$ levels are allowed. Of these, only the former transition is expected to be significant. Although experimental data on electric monopole transitions are scarce, it is worthwhile to check the predictions on the

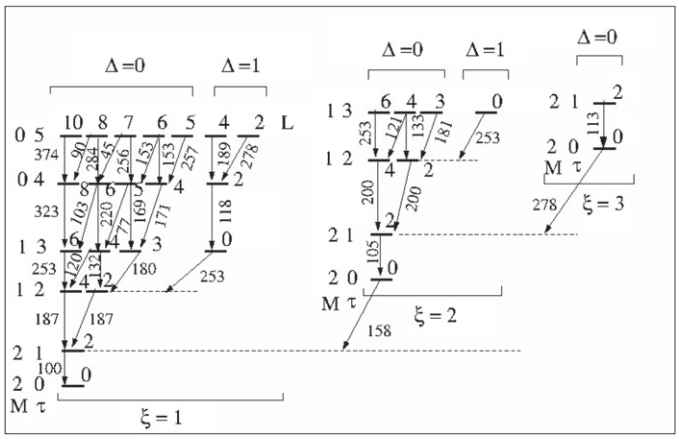

Figure 8. Benchmark numbers (energies normalized to the excitation energy of the first 2^+ and B(E2) values normalized to $B(\mathrm{E2}; 2_1^+ \to 0_1^+) = 100$) characterizing the transition from the spherical to the deformed domain within the sextic oscillator model. These quantities are fixed for any point of the critical parabola separating the two domains.

extended model on $B(\mathrm{E0}; (2,0)0^+ \to (1,0)0^+)$. Figure 10 displays this quantity in the parametric domains corresponding to figures 3 and 4. It is seen that the strength of transition falls rapidly with increasing a (roughly as $1/a$), and it is strongest when the potential has a double well structure, i.e. $b < -(15a)^{1/2}$.

3. Application to Ru and Pd nuclei

In order to demonstrate the performance of the extended model, the nuclei considered in the previous version of the model [17] seem suitable. The Ru and Pd nuclei are located near the $Z = 50$ shell closure and represent an example for the spherical to β-deformed γ-unstable phase transition. In reference [17] Cd nuclei were also discussed. However, these are omitted from the present analysis, because some of these nuclei are known to possess intruder bands [30, 31] very low in energy, which complicate the assignment of theoretical states to experimental levels and bands.

In the previous discussion of Ru and Pd nuclei [17] practically all the theoretical states with $(\xi, \tau) = (1, 1)$ (1, 2), (1, 3) and (2, 0) could be assigned to experimental levels based on their location and electric quadrupole transitions. In the extended model there are further theoretical states to which the assignment of experimental levels is relatively simple. Among these, there are the $L^\pi = 8^+$ and 10^+ members of the ground-state band, for which a cascade of E2 transitions can be observed in most nuclei. These are typically the lowest-lying experimental 8^+ and 10^+ states and their theoretical counterparts are assigned to $(\xi, \tau) = (1, 4)$ and (1, 5), respectively. The second excited states with 6^+ and 8^+ are also relatively easy to identify. Their theoretical counterparts also carry the $(\xi, \tau) = (1, 4)$ and (1, 5) quantum numbers, respectively. The lowest-lying unnatural-parity states 5^+ and 7^+ are also characteristic features of the experimental energy spectra of most nuclei, and their theoretical counterparts are those with $(\xi, \tau) = (1, 4)$ and (1, 5), respectively. In our survey we used experimental data from the national nuclear data centre [32].

Table 2. B(E2) intraband values for $\xi = 1$, normalised to $B(\mathrm{E2}; 2_1^+ \to 0_1^+)$, among all states corresponding to the sextic potential with $a = b^2/15$ with $M = 2, 1$, and 0, which is the transition line between spherical and deformed shapes (see figure 1). Each state (initial and final) is identified by the quantum numbers (ξ, τ, Δ, L).

Initial (ξ, τ, Δ, L)	$\to$	Final (ξ, τ, Δ, L)	B(E2) arb. units	Initial (ξ, τ, Δ, L)	$\to$	Final (ξ, τ, Δ, L)	B(E2) arb. units
			Intraband $\xi = 1$				
1,1,0,2		1,0,0,0	100	1,5,0,10		1,4,0,8	374
1,2,0,4		1,1,0,2	187	1,5,0,8		1,4,0,8	90
1,2,0,2		1,1,0,2	187	1,5,0,8		1,4,0,6	284
1,3,0,6		1,2,0,4	253	1,5,0,7		1,4,0,8	73
1,3,0,4		1,2,0,4	120	1,5,0,7		1,4,0,6	45
1,3,0,4		1,2,0,2	132	1,5,0,7		1,4,0,5	256
1,3,0,3		1,2,0,4	72	1,5,0,6		1,4,0,8	4
1,3,0,3		1,2,0,2	180	1,5,0,6		1,4,0,6	151
1,3,1,0		1,2,0,2	253	1,5,0,6		1,4,0,5	66
1,4,0, 8		1,3,0,6	323	1,5,0,6		1,4,0,4	153
1,4,0,6		1,3,0,6	103	1,5,0,5		1,4,0,6	27
1,4,0,6		1,3,0,4	220	1,5,0,5		1,4,0,5	90
1,4,0,5		1,3,0,6	76	1,5,0,5		1,4,0,4	257
1,4,0,5		1,3,0,4	77	1,5,1,4		1,4,0,6	30
1,4,0,5		1,3,0,3	169	1,5,1,4		1,4,0,5	124
1,4,0,4		1,3,0,6	3	1,5,1,4		1,4,0,4	31
1,4,0,4		1,3,0,4	148	1,5,1,4		1,4,1,2	189
1,4,0,4		1,3,0,3	171	1,5,1,2		1,4,0,4	96
1,4,1,2		1,3,0,4	56	1,5,1,2		1,4,1,2	278
1,4,1,2		1,3,0,3	148				
1,4,1,2		1,3,1,0	118				

The analysis of the experimental data revealed that the degeneracy of the energy eigenvalues predicted by the model for the multiplets with the same (ξ, τ) quantum numbers is not realized in the experimental spectra. The experimental levels assigned to these multiplets generally seem to follow a simple pattern: levels with higher L are higher. This situation has been handled within the sextic oscillator by including a centrifugal term with β^{-2} type dependence on β [33]. However, including such a term would complicate the formalism to the degree that the advantages of exact solvability would be lost, so we decide to apply another type of rotational term. This is the $L \cdot L$ term, which is used in algebraic models and which is diagonal in the bases used with eigenvalue $L(L+1)$. Such a term has been proposed in reference [34]. It is notable that the splitting of the energy spectrum by this term can also be attributed to other interactions, because the Casimir invariants appearing in the IBM can be expressed as the sum of scalar products of the type $A^{(j)} \cdot A^{(j)}$. The Casimir invariant of the SU(3) algebra is expressed, for example, in terms of $L \cdot L$ and $Q \cdot Q$, so the splitting of the degenerate SU(3) multiplets generated by the former operator is the same as the one generated by the latter one. In the case of O(5) and O(6) relevant to the present physical situation $L \cdot L$ appears together with other similar scalar products [2], so the splitting of the energy levels can also be attributed to residual interactions of the latter type. Considering these circumstances, we added the phenomenological $cL \cdot L$ interaction to the sextic oscillator model.

Table 3. B(E2) values, intraband $\xi = 2$ and $\xi = 3$ and interband $\xi = 2 \to \xi = 1$ and $\xi = 3 \to \xi = 2$, normalised to $B(\mathrm{E2}; 2_1^+ \to 0_1^+)$, among all states corresponding to the sextic potential with $a = b^2/15$ with $M = 2, 1$, and 0, which is the transition line between spherical and deformed shapes (see figure 1). Each state (initial and final) is identified by the quantum numbers (ξ, τ, Δ, L).

Initial (ξ, τ, Δ, L)	$\to$	Final (ξ, τ, Δ, L)	B(E2) arb. units	Initial (ξ, τ, Δ, L)	$\to$	Final (ξ, τ, Δ, L)	B(E2) arb. units
			Intraband $\xi = 2$				
2,1,0,2		2,0,0,0	105	2,3,0,4		2,2,0,2	133
2,2,0,4		2,1,0,2	200	2,3,0,3		2,2,0,4	72
2,2,0,2		2,1,0,2	200	2,3,0,3		2,2,0,2	181
2,3,0,6		2,2,0,4	253	2,3,1,0		2,2,0,2	253
2,3,0,4		2,2,0,4	121				
			Interband $\xi = 2 \to \xi = 1$				
2,0,0,0		1,1,0,2	158	2,2,0,4		1,3,0,6	64
2,1,0,2		1,2,0,4	53	2,1,0,2		1,2,0,2	29
2,2,0,4		1,3,0,4	21	2,2,0,2		1,3,0,4	42
2,2,0,4		1,3,0,3	10	2,2,0,2		1,3,1,0	9
2,2,0,2		1,3,0,3	42	2,3,0,6		1,4,0,6	10
2,3,0,6		1,4,0,8	40	2,3,0,6		1,4,0,4	0.2
2,3,0,6		1,4,0,5	6	2,3,0,4		1,4,0,5	9
2,3,0,4		1,4,0,6	30	2,3,0,4		1,4,1,2	3
2,3,0,4		1,4,0,4	14	2,3,0,3		1,4,0,4	21
2,3,0,3		1,4,0,5	25	2,3,1,0		1,4,1,2	2
2,3,0,3		1,4,1,2	10				
			Intraband $\xi = 3$				
3,0,0,2		3,1,0,0	113				
			Interband $\xi = 3 \to \xi = 2$				
3,0,0,0		2,1,0,2	278	3,1,0,2		2,2,0,4	98
3,1,0,2		2,2,0,2	54				

After identifying these levels, the energy spectrum of each nucleus was obtained using a two-step procedure. In the first step, the energy eigenvalues of these states were fitted with the theoretical excitation energy as in equation (38), and a set of parameters a, b and c were extracted. In the second step, further experimental states were assigned to theoretical levels, based on their location and, whenever possible, their electric quadrupole transitions. In both stages of the fitting procedure specific weights were assigned to the levels. In order to avoid overrepresenting less well-known higher-lying states, the weight of unity (1) was distributed evenly among the levels supposed to belong to the same (ξ, τ) multiplet. In this way, the members of the (1, 2), (1, 3), (1, 4) and (1, 5) multiplets carried the weight 1/2, 1/4, 1/5 and 1/7, respectively, while the states that stood alone in their multiplet (e.g. $2^+(1, 1), 0^+(2, 0), 2^+(2, 1)$, $0^+(3, 0)$ and $2^+(3, 1)$ had weight 1. In case the experimentally observed spin-parity of these states was ambiguous, then its weight calculated as above, was halved.

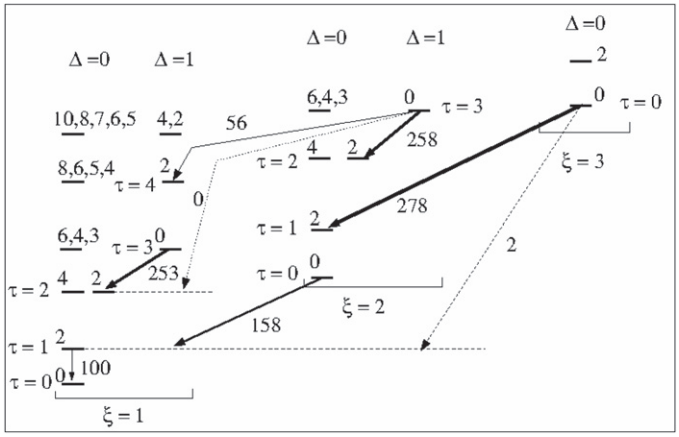

Figure 9. Benchmark numbers for B(E2) values involving the low-lying $L^\pi = 0^+$ states normalized to $B(\mathrm{E2}; 2_1^+ \to 0_1^+) = 100$ and characterizing the transition from the spherical to the deformed domain within the sextic oscillator model. These quantities are fixed for any point of the critical parabola separating the two domains.

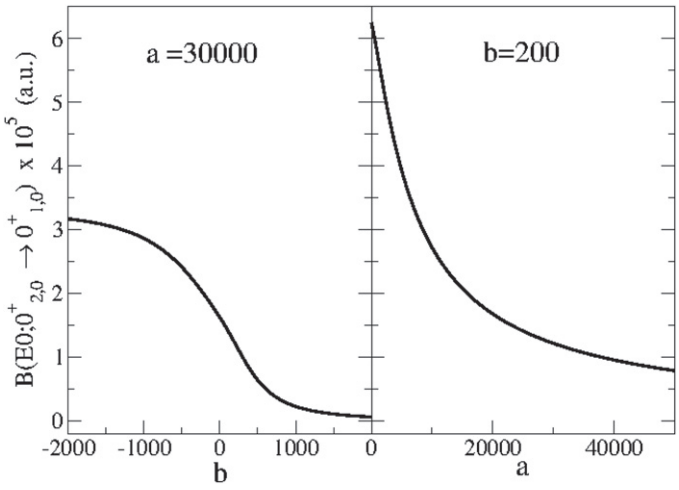

Figure 10. The strength of the electric monopole transition from the $(\xi, \tau)L^\pi = (2, 0)0^+$ bandhead state to the $(1, 0)0^+$ ground state for selected parameter domains.

The result of the fitting procedure is presented in tables 4 and 5, for Ru and Pd isotopes, respectively. Missing entries indicate theoretical levels with unidentified experimental counterparts. These include typically high-lying low-spin states, including some with 0^+, and some unnatural-parity states. To estimate the quality of the fits, the weighted root mean square deviation values $D = [(N\sum_{i=1}^{N} w_i(E_{xi}^{\mathrm{Th}} - E_{xi}^{\mathrm{Exp}})^2/(N-1)\sum_{i=1}^{N} w_i]^{1/2}$ were calculated and are displayed in the last row. This value is in the same range (roughly within a factor of two) for both isotope chains. For the Ru isotopes it is somewhat higher for the lighter isotopes, where the number of fitted states is higher due to the more abundant data set. In contrast, for the Pd isotopes D is the largest for the lightest isotope, ^{102}Pd, which has the least complete data set.

Table 4. Experimental (E_x^{Exp}) [32] and theoretical (E_x^{Th}) energy eigenvalues for the Ru isotopes displayed in keV as ($E_x^{\mathrm{Exp}}/E_x^{\mathrm{Th}}$). E_x^{Exp} in parenthesis indicates uncertain L^π assignment. An asterisk in front of $(\xi,\tau)L^\pi$ signifies that the given level was considered in the first round of the fitting procedure (see the text for details). The potential parameters a, b and c fitted with the wider set of levels are displayed in the last section, followed by the weighted root mean square deviation, D.

$(\xi,\tau)L^\pi$	^{98}Ru	^{100}Ru	^{102}Ru	^{104}Ru	^{106}Ru	^{108}Ru
$*(1,1)2^+$	652/671	540/635	475/562	358/372	270/320	242/287
$*(1,2)2^+$	1414/1313	1362/1220	1103/1079	893/893	792/748	(708)/607
$*(1,2)4^+$	1398/1413	1226/1351	1106/1203	889/989	(715)/819	665/733
$*(1,3)0^+$	(2371)/1901	1741/1743	1837/1537	1335/1240	./1079	./866
$*(1,3)3^+$	1797/1987	1881/1856	1522/1643	1242/1321	(1092)/1141	(975)/974
$*(1,3)4^+$	2267/2044	2063/1931	1799/1714	1503/1376	(1307)/1181	(1183)/1046
$*(1,3)6^+$	2223/2201	2074/2138	1873/1908	1556/1526	(1296)/1294	1241/1244
$(1,4)2^+$	(2468)/2595	2544/2390	./2113	2035/1915	(1774)/1671	./1376
$(1,4)4^+$	(2720)/2695	(2512)/2521	(2442)/2237	2081/2011	./1742	(1644)/1502
$*(1,4)5^+$	2547/2766	(2577)/2615	2219/2326	(1872)/2079	(1641)/1793	(1496)/1592
$*(1,4)6^+$	(2867)/2852	2706/2728	2587/2432	(2197)/2160	(1908)/1855	(1762)/1700
$*(1,4)8^+$	3127/3066	3060/3009	2706/2697	2320/2365	(1973)/2008	1942/1970
$(1,5)2^+$	(3367)/3229	3072/2971	./2626	2285/2344	./2083	./1743
$(1,5)4^+$	(3523)/3329	3065/3102	(2719)/2750	./2439	./2155	./1869
$(1,5)5^+$	(3251)/3400	(2661)/3196	./2838	./2507	./2206	(1826)/1959
$(1,5)6^+$	(3579)/3486	./2309	./2944	./2589	./2267	./2067
$*(1,5)7^+$	(3284)/3586	(3576)/3440	3035/3068	(2623)/2684	(2284)/2339	(2133)/2194
$*(1,5)8^+$	./3700	(3550)/3591	(3395)/3210	(2848)/2793	./2420	(2420)/2338
$*(1,5)10^+$	4001/3971	4083/3947	3434/3546	3112/3052	2705/2614	2741/2680
$*(2,0)0^+$	1322/1278	1130/1167	944/1031	988/1021	991/967	(976)/888
$(2,1)2^+$	1817/1955	1865/1805	1581/1597	1515/1500	1392/1423	(1249)/1321
$(2,2)2^+$	(2427)/2608	2241/2397	2037/2122	(2095)/2151	(1886)/1989	./1764
$(2,2)4^+$	(2812)/2708	(2414)/2528	(2420)/2246	(2269)/2246	./2061	./1891
$(2,3)0^+$	./3203	./2923	(2676)/2584	./2579	(2633)/2422	./2133
$(2,3)3^+$	(3442)/3288	(3110)/3036	(2701)/2690	./2661	./2483	./2241
$(2,3)4^+$	(3475)/3346	./3111	(3202)/2761	./2716	./2524	./2313
$(2,3)6^+$	(3539)/3503	./3317	./2955	./2865	./2636	./2511
$(3,0)0^+$	(2670)/2573	2387/2344	(1968)/2074	./2242	./2141	./1938
$(3,1)2^+$	(3205)/3256	./2985	./2644	./2799	./2694	./2482
a (nat. u.)	246.4	112.6	131.4	3340.1	4083.9	4147.6
b (nat. u.)	317.0	290.7	256.3	196.7	151.1	95.0
c (keV)	7.14	9.39	8.85	6.81	5.11	9.00
D (keV)	127	105	120	63	70	75

It is worth mentioning that the quality of our fits for Ru and Pd are similar to those obtained in the numerical work presented in reference [24], although a direct comparison is not possible, because we have included the $L \cdot L$ term.

The resulting potential parameters exhibit characteristic behaviour. Figure 11 displays the two isotope chains located on the (a, b) phase space. The lighter members of the Ru chain are close to the b axis, meaning that they are close to the harmonic oscillator approximation. Then a begins to increase, while b continues to decrease, and this pattern means that the trajectory crosses the critical parabola $a = b^2/15$ with ^{104}Ru, then continues with a roughly constant a value up to ^{108}Ru. This is rather similar to the behaviour observed for the limited model in

Table 5. The same as table 4, for the Pd isotopes.

$(\xi,\tau)L^{\pi}$	^{102}Pd	^{104}Pd	^{106}Pd	^{108}Pd	^{110}Pd
$*(1,1)2^{+}$	556/527	556/611	512/544	434/412	374/351
$*(1,2)2^{+}$	1534/1328	1342/1281	1128/1113	931/952	814/819
$*(1,2)4^{+}$	1276/1371	1324/1391	1229/1246	1048/1073	921/942
$*(1,3)0^{+}$	1658/1902	1793/1822	1706/1562	1314/1301	1171/1101
$*(1,3)3^{+}$	2112/1939	(1821)/1916	1558/1676	1335/1404	(1212)/1207
$*(1,3)4^{+}$	2138/1963	2082/1979	1932/1751	(1624)/1473	1398/1277
$*(1,3)6^{+}$	2111/2031	2250/2152	2077/1960	1771/1663	1574/1471
$(1,4)2^{+}$	(2716)/2894	2521/2600	2309/2236	(2099)/1981	1470/1704
$(1,4)4^{+}$	(2799)/2937	2678/2711	2351/2369	1956/2102	1718/1827
$*(1,4)5^{+}$	(2977)/2967	(2924)/2789	2366/2463	2084/2188	(1759)/1915
$*(1,4)6^{+}$	(3002)/3004	(3112)/2884	./2577	(2421)/2291	(1987)/2020
$*(1,4)8^{+}$	3013/3096	3220/3120	2963/2961	2548/2550	2296/2284
$(1,5)2^{+}$	./3549	(3214)/3209	2821/2758	2391/2412	2141/2068
$(1,5)4^{+}$	./3591	3284/3319	./2890	2540/2533	(2089)/2191
$(1,5)5^{+}$	./3622	./3398	2951/2985	(2671)/2619	(2261)/2279
$(1,5)6^{+}$	./3659	./3492	./3099	(2709)/2723	(2335)/2384
$*(1,5)7^{+}$	./3702	./3602	./3231	(2919)/2843	./2508
$*(1,5)8^{+}$	(3340)/3751	(3422)/3728	./3383	(2954)/2981	(2651)/2649
$*(1,5)10^{+}$	3993/3867	4023/4028	3534/3742	3257/3309	(2903)/2983
$*(2,0)0^{+}$	1593/1562	1334/1297	1134/1105	1053/1012	947/873
$(2,1)2^{+}$	(2391)/2251	(1999)/1955	1562/1685	1441/1501	1214/1296
$(2,2)2^{+}$	(3123)/3249	2695/2703	2242/2315	2218/2147	1890/1861
$(2,2)4^{+}$	(3166)/3292	2801/2813	2649/2448	./2268	1934/1984
$(2,3)0^{+}$	./3948	./3285	2828/2796	./2558	./2201
$(2,3)3^{+}$	./3985	(3408)/3379	(2851)/2910	./2661	./2306
$(2,3)4^{+}$	./4009	3474/3442	./2986	(2864)/2730	./2377
$(2,3)6^{+}$	./4076	(3310)/3615	./3194	./2920	(2775)/2570
$(3,0)0^{+}$	./3430	./2712	2278/2303	./2188	./1896
$(3,1)2^{+}$	./4236	./3410	2918/2914	2720/2736	2370/2373
a (nat. u.)	7722.3	1874.4	1235.7	2372.5	1929.1
b (nat. u.)	302.8	304.2	260.9	215.6	182.0
c (keV)	3.06	7.87	9.47	8.62	8.80
D (keV)	133	82	90	61	81

reference [17], with the exception that the crossing of the critical parabola (which lies slightly higher there, $a = b^2/11$) occurs between ^{104}Ru and ^{106}Ru.

Interestingly, the Pd chain follows a different trajectory. The b parameter also decreases with increasing A, however, the a parameter has a different behaviour, leading to a trajectory that is more or less parallel with the critical parabola. This is also somewhat similar to the situation observed for the limited model in reference [17]. It has to be noted though, that the fits there were made in an analytic way, as the a and b parameters were extracted from the relative position of energy levels $0^{+}(2,0)$ and $2^{+}(1,2)$. Whenever the former state fell below the latter one, the a parameter acquired a negative value, which would have led to unnormalizable wavefunctions. In order to avoid this situation, in reference [17] the $a = 0$ choice was made, leading to the harmonic oscillator approximation. In the present analysis, at the same time, both a and b were extracted from a numerical fit, so an a value close to 0 is not based on a technical choice.

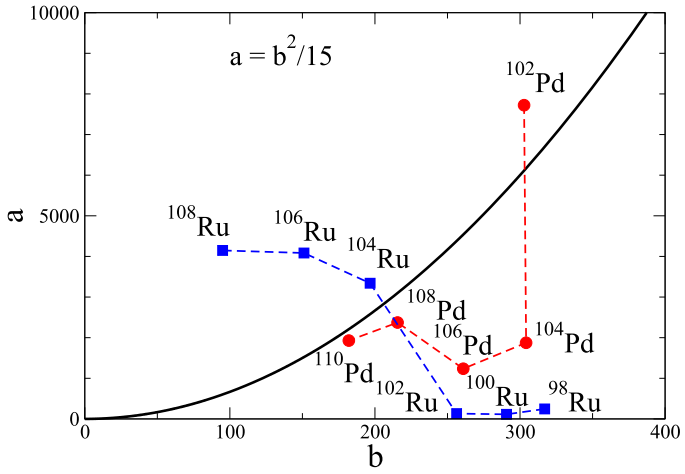

Figure 11. The location of the Ru and Pd nuclei in the (a, b) phase space based on the fitted a and b parameter values.

Another difference between the present analysis and that in reference [17] is the presence of the phenomenological rotational term. As it can be seen from tables 4 and 5, the variation of the c rotational parameter is quite smooth for both chains, and c is close to a common value except for ^{102}Pd. (In the case of this nucleus there are several missing assignments in the $E_x > 3500$ keV domain, where the experimental spectrum contains positive-parity only levels with $L > 8$.) Omitting the phenomenologic rotational term results in a and b parameters that are close to those obtained in reference [17] using the simpler version of the model. Forcing the members of the (ξ, τ) multiplets at the same degenerate energy value typically does not influence much the location of the theoretical energy levels with low value of L, while the largest differences compared to the experimental energy levels occur for the 10^+ and 8^+ levels, which are predicted to be lower than the experimental states.

As particular example to demonstrate the performance of the extended model, the ^{108}Pd nucleus is chosen, which is close to the critical parabola, and for which a relatively extensive set of electric quadrupole transition data is available. Figure 12 displays the experimental and theoretical energy eigenvalues (as in table 5), together with the B(E2) values between the levels. Most of the experimental levels could be assigned to theoretical states. The missing cases are $(\xi, \tau)L^\pi = (2, 2)4^+$, $(2, 3)0^+$, 3^+, 6^+ and $(3, 0)0^+$ in the $E_x = 2200$–3000 keV range. There are, however, several experimental levels in this region without L^π assignment, for which information is available on which low-lying states they decay to [32]. The level at $E_x = 2404$ keV, for example, is known to decay to the 2_1^+ state, so it could be a candidate for the $(3, 0)0^+$ theoretical state (see figure 9). A candidate for the $(2, 2)4^+$ theoretical level could be the level at $E_x = 2282.43$, which decays to the 3_1^+ level, which correspond to the theoretical level $(\xi, \tau)L^\pi = (1, 3)3^+$, representing a transition that is allowed in the present scheme.

The experimental B(E2) values are reproduced reasonably well: the theoretical B(E2) values between $\xi = 1$ states are typically 20 to 30 percent stronger than the experimental value. Exceptions are the $(4^+)(1624) \to 4^+(1048)$ and $0^+(1314) \to 2^+(931)$ transitions, which are substantially stronger. Theoretical transition strengths from the $\xi = 2$ states are typically 50 percent stronger than the experimental values. A major discrepancy is the transition from

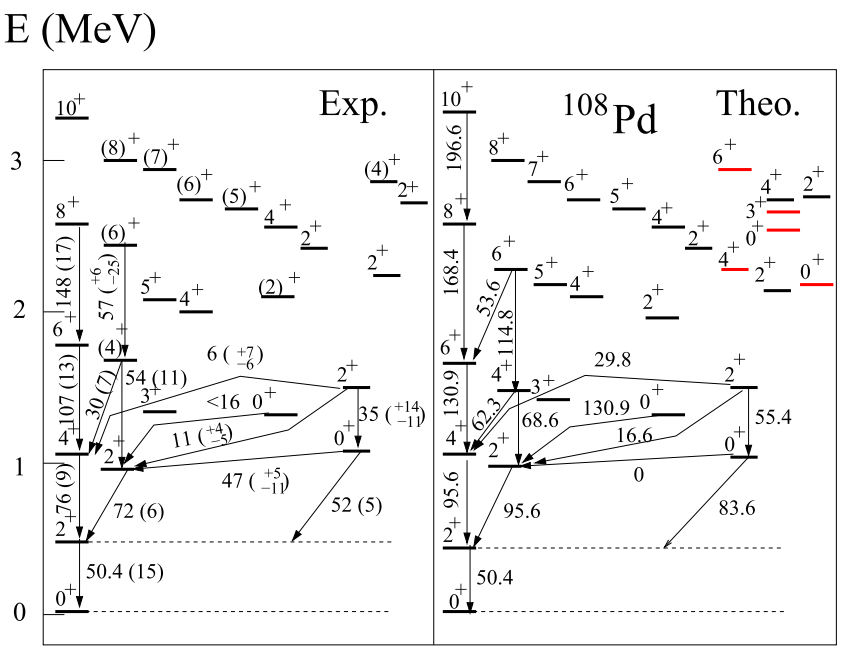

Figure 12. Spectroscopic properties of the ^{108}Pd nucleus and their interpretation in terms of the extended sextic oscillator model. Theoretical E2 transitions are normalized to the mean experimental value $B(\mathrm{E2}; 2_1^+ \to 0_1^+) = 50.4$ W.u. Data are taken from reference [32]. Theoretical energy levels indicated in red are predicted $\xi = 2$ and 3 levels without experimentally assigned partners (see the text).

the $0^+(1053)$ bandhead to the $2^+(931)$ level, which should be forbidden, while the experimental B(E2) value is comparable to that of the allowed transition to the $2^+(434)$ level. It should be noted that here the simplest E2 operator (linear in β), equation (40), is used and this obeys the $\Delta\tau = 1$ rule. However, the introduction of higher order terms in the E2 operator will break that rule [35]. Another indication for the reasonable performance of the model is that there are about ten transitions (not shown in figure 12) with less than 5 percent of the strength of the $2_1^+ \to 0_1^+$ transition, which are all forbidden in the present scheme.

3.1. Error estimates of the model

In the last few years there has been an increasing interest in providing error estimates for the theoretical calculations obtained from models that depend on several parameters. Here we follow the ideas put forward in reference [37], where it was proposed that in the fitting of energy eigenvalues, varying weights can be assigned to the energy levels depending on their importance. In addition, we also follow reference [38] for the error estimate of energies and B(E2) values.

We present the error estimates for the case of ^{108}Pd studied above in detail. As discussed in the manuscript, weights were assigned to the energy levels such that (1) $w = 1$ was distributed evenly among states belonging to the same τ multiplet, by which the most important (mainly) bandhead states were taken into account with higher priority, and (2) the weight of energy

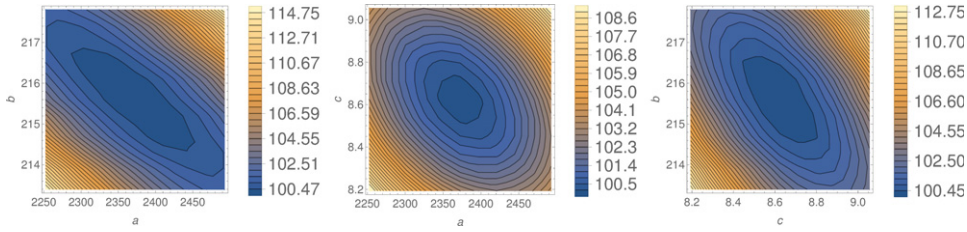

Figure 13. The contour plots for χ^2 with projections on the plane a–b (left panel), a–c (middle panel), and c–b (right panel). For the purpose of these plots χ^2-values have been normalised to 100 at the minimum, located at $(a_0, b_0, c_0) = (2372.5, 215.62, 8.6236)$ for ^{108}Pd.

levels with uncertain spin-parity assignment was halved. This is in line with the practice outlined in reference [37]. Then, a χ^2 function was constructed and the best fit provided with the parameters that minimise the χ^2 function (a_0, b_0, c_0). In the ^{108}Pd case the best fit parameters are $(a_0 = 2372.5, b_0 = 215.6, c_0 = 8.624)$. Around this minimum the function is accepted to have a parabolic behaviour in the three parameters,

$$\chi^2(a,b,c) = \chi^2(a_0,b_0,c_0) + ((a-a_0)\ (b-b_0)\ (c-c_0)) \times \begin{pmatrix} M_{aa} & M_{ab} & M_{ac} \\ M_{ab} & M_{bb} & M_{bc} \\ M_{ac} & M_{bc} & M_{cc} \end{pmatrix} \begin{pmatrix} (a-a_0) \\ (b-b_0) \\ (c-c_0) \end{pmatrix}. \tag{44}$$

Then, one can make a grid of points in the range $(a_0 \pm \Delta a, b_0 \pm \Delta b, c_0 \pm \Delta c)$ around the minimum for $\chi^2(a_0, b_0, c_0) = \chi_0^2$. The first question is how to select a reasonable domain $(\Delta a, \Delta b, \Delta c)$ of the model parameters. In our case, following reference [38], we obtained $(\Delta a = 0.05a_0, \Delta b = 0.01b_0, \Delta c = 0.05c_0) \approx (120, 2.2, 0.4)$. In figure 13 we present contour plots of the χ^2 values, in the a–b, a–c and c–b planes, around the minimum. For this purpose, we have normalised the minimum χ_0^2 value to 100. Lines inside the figures mark points with the same χ^2 value.

These figures give some information on the uncertainties in the model parameters and on the parameter correlations. This information can be made quantitative by determining the $\hat{M}-$matrix in equation (44) by using the points in the selected domain of parameters. In our case for ^{108}Pd and for the χ^2 distribution with a value 100 at the minimum, we obtain the following $\hat{M}$ matrix,

$$\hat{M} = \begin{pmatrix} 0.000\,106\,283 & 0.005\,438\,61 & -0.013\,517 \\ 0.005\,438\,61 & 0.565\,867 & 0.237\,598 \\ -0.013\,5171 & 0.237\,598 & 6.342\,16 \end{pmatrix}. \tag{45}$$

From this matrix, one can obtain the covariance matrix $\hat{C}$ just taking the inverse of $\hat{M}$ and multiply by the corresponding scale factor s [38], that in our case is approx $s = 100/23 \approx 4$. Thus, the covariance matrix in our case is

$$\hat{C} = s\hat{M}^{-1} = \begin{pmatrix} 285348. & -3045.78 & 722.268 \\ -3045.78 & 39.6921 & -7.97848 \\ 722.268 & -7.978\,48 & 2.468\,97 \end{pmatrix}. \tag{46}$$

Table 6. Estimation of the error (uncertainty) assigned to the theoretical energy eigenvalues determined for ^{108}Pd.

State (ξ, τ, L)	E_x^{Exp}	E_x^{Th}	Estimated error	Weight
(1, 1, 2)	434	412	±21	1.00
(1, 2, 2)	931	952	±12	0.50
(1, 2, 4)	1048	1073	±26	0.50
(1, 3, 0)	1314	1301	±31	0.25
(1, 3, 3)	1335	1404	±20	0.25
(1, 3, 4)	1624	1473	±21	0.12
(1, 3, 6)	1771	1663	±47	0.25
(1, 4, 2)	2099	1981	±27	0.10
(1, 4, 4)	1956	2102	±44	0.20
(1, 4, 5)	2084	2188	±58	0.20
(1, 4, 6)	2421	2291	±77	0.10
(1, 4, 8)	2548	2550	±123	0.20
(1, 5, 2)	2391	2412	±25	0.14
(1, 5, 4)	2540	2533	±38	0.14
(1, 5, 5)	2671	2619	±51	0.07
(1, 5, 6)	2709	2723	±68	0.07
(1, 5, 7)	2919	2843	±89	0.07
(1, 5, 8)	2954	2981	±114	0.07
(1, 5, 10)	3257	3309	±172	0.14
(2, 0, 0)	1053	1012	±25	1.00
(2, 1, 2)	1441	1501	±27	1.00
(2, 2, 2)	2218	2147	±63	0.50
(2, 2, 4)		2268	±82	0.00
(2, 3, 0)		2558	±52	0.00
(2, 3, 3)		2661	±68	0.00
(2, 3, 4)	2864	2730	±79	0.12
(2, 3, 6)		2920	±111	0.00
(3, 0, 0)		2188	±77	0.00
(3, 1, 2)	2720	2736	±89	1.00

This $\hat{C}$ matrix provides with the standard deviations of the model parameters

$$\hat{C} = \begin{pmatrix} \sigma_{aa}^2 & \sigma_{ab}^2 & \sigma_{ac}^2 \\ \sigma_{ab}^2 & \sigma_{bb}^2 & \sigma_{bc}^2 \\ \sigma_{ac}^2 & \sigma_{bc}^2 & \sigma_{cc}^2 \end{pmatrix}. \tag{47}$$

From these results one obtains $\sigma_{aa} = 534$, $\sigma_{bb} = 6$, $\sigma_{cc} = 1.6$, $\sigma_{ab}^2 = -3046$, $\sigma_{ac}^2 = 722$, and $\sigma_{bc}^2 = -8$. With this information we can estimate the errors of any observable that depends on the model parameters with the usual error propagation,

$$\sigma_{\hat{O}(a,b,c)}^2 = \left(\left. \frac{\partial \hat{O}}{\partial a} \right|_{a_0,b_0,c_0} \right)^2 \sigma_{aa}^2 + \left(\left. \frac{\partial \hat{O}}{\partial b} \right|_{a_0,b_0,c_0} \right)^2 \sigma_{bb}^2 + \left(\left. \frac{\partial \hat{O}}{\partial c} \right|_{a_0,b_0,c_0} \right)^2 \sigma_{cc}^2 + 2 \left(\left. \frac{\partial \hat{O}}{\partial a} \right|_{a_0,b_0,c_0} \right) \left(\left. \frac{\partial \hat{O}}{\partial b} \right|_{a_0,b_0,c_0} \right) \sigma_{ab}^2$$

Table 7. Experimental and theoretical B(E2) values for ^{108}Pd appearing in figure 12. The experimental errors and the estimation of the uncertainty assigned to the theoretical energy eigenvalues are also displayed.

Initial state	Final state	$B(\mathrm{E2})_{\mathrm{Exp.}}$	$B(\mathrm{E2})_{\mathrm{Th.}}$
$(\xi,\tau,L)_i$	$(\xi,\tau,L)_f$	(W.u.)	(W.u.)
(1, 1, 2)	(1, 0, 0)	50.4 ±1.5	50.4 ±1.1
(1, 2, 4)	(1, 1, 2)	76 ±9	95.6 ±1.2
(1, 3, 6)	(1, 2, 4)	107 ±13	130.9 ±1.6
(1, 4, 8)	(1, 3, 6)	148 ±17	168 ±3
(1, 5, 10)	(1, 4, 8)		197 ±5
(1, 2, 2)	(1, 1, 2)	72 ±6	95.6 ±1.2
(1, 3, 0)	(1, 2, 2)	< 16	130.9 ±1.6
(1, 3, 4)	(1, 2, 4)	30 ±7	62.3 ±1.0
(1, 3, 4)	(1, 2, 2)	54 ±11	68.6 ±1.0
(1, 4, 6)	(1, 3, 6)		53.6 ±1.0
(1, 4, 6)	(1, 3, 4)	57^{+6}_{-25}	115 ±2
(2, 1, 2)	(2, 1, 0)	35^{+14}_{-11}	55.4 ±1.4
(2, 0, 0)	(1, 1, 2)	52 ±5	83 ±2
(2, 1, 2)	(1, 2, 4)	6^{+7}_{-6}	30 ±3
(2, 1, 2)	(1, 2, 2)	11^{+4}_{-5}	16.6 ±1.5

$$+2\left(\frac{\partial\hat{O}}{\partial a}\bigg|_{a_0,b_0,c_0}\right)\left(\frac{\partial\hat{O}}{\partial c}\bigg|_{a_0,b_0,c_0}\right)\sigma_{ac}^2$$
$$+2\left(\frac{\partial\hat{O}}{\partial b}\bigg|_{a_0,b_0,c_0}\right)\left(\frac{\partial\hat{O}}{\partial c}\bigg|_{a_0,b_0,c_0}\right)\sigma_{bc}^2\ . \tag{48}$$

The partial derivatives can be estimated numerically. (In the case of models with parameters that appear in the Hamiltonian in a linear form, e.g. various algebraic models, it is possible to carry out the error estimation fully analytically.) Finally, one can obtain the estimated errors for any observable using the $\hat{C}-$ matrix and equation (48).

In the case of ^{108}Pd the estimated errors for the energies are given in table 6 together with the state labels and weights assigned. It is seen that in two-thirds of the cases the difference of the experimental and calculated energy eigenvalue is within the estimated theoretical error of the given energy level, and there is only one level for which this difference is larger than the double of the estimated error.

The same procedure can be used to assign errors to the calculated B(E2) values. In this case, the observable does not depend on c, only on parameters (a, b). The results for ^{108}Pd are given in table 7.

The estimated theoretical error is in the range of 1 to 2 percents of the mean B(E2) value, except for two transitions from the $(\xi,\tau)L^\pi = (2,1)2^+$ state. Note that this is below the 3 percent error originating from the propagation of the experimental error of the reference transition strength.

4. Summary

Within the BM model the interaction potential is in general a function of the shape variables (β, γ). Solution of the Bohr equation with general potentials is usually very involved, but for particular selections of the potential it can be solved exactly, at least for a set of low-lying states. These cases are very important since they provide simple analytic solution for a complex problem and, in addition, they give precise numbers against which more involved calculations can be checked. One of these cases is the γ-unstable potential with a sextic β-dependence. This type of potential is part of the family known as QES potentials (QES). In this case one can find exact solutions for the states in the lowest energy region of the system. The number of exact solutions depends on M, the degree of the polynomial part of the wavefunctions. Increasing M allows to have more solutions with the drawback that for larger M one has to apply numerical techniques to determine the coefficients of the polynomial component of the wavefunction.

In a couple of previous papers [16, 17] the case for $M = 0$, and 1 was solved for the γ-unstable potential with a sextic β-dependence. This allowed to obtain exact results for τ up to three and a total of 10 lowest-lying states with maximum angular momentum $L = 6$. Here, an extension of the same problem to include $M = 0, 1$, and 2 is worked out. For $M = 2$ the exact solutions were generated by solving a cubic algebraic equation, which was feasible using the Cardano formula. This allows to study states up to $\tau = 5$, in such a way that 30 low-lying states, with maximum angular momentum up to $L = 10$, are obtained. This extension is important for describing actual nuclei and for analysis of shape phase transitions since allows more observables to be checked. However, for using the model in spectroscopic studies, the degeneracy in τ for different L values has to be removed since it is not observed experimentally. Here a phenomenological $L \cdot L$ term has been proposed for this.

The Pd–Ru region of the nuclear chart has been studied with the extended model with good results. In addition, the shape phase transitions in these isotopic chains have been studied again with much more data and the obtained results are consistent with those presented in reference [17]. The model space depends on two parameters that define the potential (a, b), and the full space is divided in three regions by a critical parabola. The three γ-unstable shapes are: one spherical, one deformed, and one with two coexisting minima (one spherical and another deformed). The model provides specific numbers for energy ratios and for B(E2) transition values at the critical parabola. For the case of the isotope chains studied, Ru isotopes provide a clear example of transition from spherical to deformed and ^{104}Ru seems to be the closest to criticality. The Pd isotopes were found to have spherical minimum, but some are not far from criticality. One of them is ^{108}Pd, which we discussed in more detail, showed that its spectroscopic properties are close to the benchmark values of the model.

Acknowledgments

This work was partially supported by the National Research, Development and Innovation Office (NKFIH), Grant No. K112962, by the Consejería de Economía, Conocimiento, Empresas y Universidad de la Junta de Andalucía (Spain) under Group FQM-160, by the Spanish Ministerio de Ciencia e Innovaciíon, ref. FIS2017-88410-P and PID2019-104002GB-C22, and by the European Commission, ref. H2020-INFRAIA-2014-2015 (ENSAR2).

Appendix A. Radial integrals for the sextic oscillator for $M = 2$

The integrals necessary to calculate matrix elements with the sextic oscillator wavefunctions contain the following expression:

$$\begin{aligned} I^{(A)} &= \int_0^\infty \beta^A \exp\left(-\frac{a}{2}\beta^4 - b\beta^2\right) \mathrm{d}\beta \\ &= \frac{1}{2}\Gamma\left(\frac{A+1}{2}\right)(2a)^{-(A+1)/4} U\left(\frac{A+1}{4}, \frac{1}{2}; \frac{b^2}{2a}\right) \\ &\equiv \frac{1}{2}\Gamma\left(\frac{A+1}{2}\right)(2a)^{-(A+1)/4} U_{A+1}. \end{aligned} \tag{A.1}$$

This is valid for $a > 0$. For $a = 0$ and $b > 0$ the problem reduces to the harmonic oscillator and the wavefunctions are the harmonic oscillator wavefunctions, so everything can be taken from the standard treatment of that problem. Similar integrals were presented in reference [17], where a minor error occurred in equation (11) in the power of $2a$. In (A.1) U_{A+1} is just a shorthand notation for an expression that occurs frequently in the formulas.

The $U(s, t; z)$ functions are one type of the confluent hypergeometric function, and their actual form appearing in the forthcoming formulas can be expressed as (see equation 13.1.3 in reference [36]);

$$U\left(s, \frac{1}{2}, z\right) = \frac{\pi^{1/2}}{\Gamma\left(a + \frac{1}{2}\right)}\, {}_1F_1\left(s, \frac{1}{2}; z\right) - \frac{2\pi^{1/2}}{\Gamma(a)}\, {}_1F_1\left(s + \frac{1}{2}, \frac{3}{2}; z\right). \tag{A.2}$$

Taking the general matrix elements of the operator β^δ with the wavefunctions (9) and applying (A.1), one finds using the shorthand notation $U_x \equiv U(\frac{x}{4}, \frac{1}{2}; \frac{b^2}{2a})$ that

$$\begin{aligned} W^\delta_{\alpha,\gamma} &\equiv \int_0^\infty \phi_\gamma(\beta)\beta^\delta\phi_\alpha(\beta)\mathrm{d}\beta \\ &= N_\alpha N_\gamma \frac{1}{2}\Gamma\left(\frac{\tau_\alpha + \tau_\gamma + \delta + 5}{2}\right)(2a)^{-(\tau_\alpha+\tau_\gamma+\delta+13)/4} \\ &\quad \times \left[(2a)^2 U_{\tau_\alpha+\tau_\gamma+\delta+5} + \frac{\tau_\alpha + \tau_\gamma + \delta + 5}{2}(2a)^{3/2}(d_\alpha + d_\gamma)U_{\tau_\alpha+\tau_\gamma+\delta+7}\right. \\ &\quad + \left(\frac{\tau_\alpha + \tau_\gamma + \delta + 5}{2}\right)_2 (2a)(d_\alpha d_\gamma + g_\alpha + g_\gamma)U_{\tau_\alpha+\tau_\gamma+\delta+9} \\ &\quad + \left(\frac{\tau_\alpha + \tau_\gamma + \delta + 5}{2}\right)_3 (2a)^{1/2}(d_\alpha g_\gamma + g_\alpha d_\gamma)U_{\tau_\alpha+\tau_\gamma+\delta+11} \\ &\quad \left. + \left(\frac{\tau_\alpha + \tau_\gamma + \delta + 5}{2}\right)_3 g_\alpha g_\gamma U_{\tau_\alpha+\tau_\gamma+\delta+13}\right]. \end{aligned} \tag{A.3}$$

Here $(x)_n = \Gamma(x + n)/\Gamma(x)$ is Pochhammer's symbol.

The normalization constants can be determined from (A.3) by calculating $W^0_{\alpha,\alpha}$, i.e. considering $\delta = 0$ and $\alpha = \gamma$. The result is

$$N_\alpha = (2a)^{(2\tau_\alpha+13)/8}\left(\frac{2}{\Gamma\left(\tau_\alpha+\frac{5}{2}\right)}\right)^{1/2}\left[(2a)^2U_{2\tau_\alpha+5}+\left(\tau_\alpha+\frac{5}{2}\right)(2a)^{3/2}2d_\alpha U_{2\tau_\alpha+7}\right.$$
$$+\left(\tau_\alpha+\frac{5}{2}\right)_2(2a)(d_\alpha^2+2g_\alpha)U_{2\tau_\alpha+9}+\left(\tau_\alpha+\frac{5}{2}\right)_3(2a)^{1/2}2d_\alpha g_\alpha U_{2\tau_\alpha+11}$$
$$\left.+\left(\tau_\alpha+\frac{5}{2}\right)_4 g_\alpha^2 U_{2\tau_\alpha+13}\right]^{-1/2}. \tag{A.4}$$

The actual normalization constants can be obtained after substituting the appropriate values of d_α and g_α for each α and γ from table 1.

The matrix elements of the linear E2 operator can be obtained from equation (A.3) by taking $\delta = 1$:

$$W^1_{\alpha,\gamma} = N_\alpha N_\gamma \frac{1}{2}\Gamma\left(\frac{\tau_\alpha+\tau_\gamma+6}{2}\right)(2a)^{-(\tau_\alpha+\tau_\gamma+14)/4}$$
$$\times\left[(2a)^2U_{\tau_\alpha+\tau_\gamma+6}+\frac{\tau_\alpha+\tau_\gamma+6}{2}(2a)^{3/2}(d_\alpha+d_\gamma)U_{\tau_\alpha+\tau_\gamma+8}\right.$$
$$+\left(\frac{\tau_\alpha+\tau_\gamma+6}{2}\right)_2(2a)(d_\alpha d_\gamma+g_\alpha+g_\gamma)U_{\tau_\alpha+\tau_\gamma+10}$$
$$+\left(\frac{\tau_\alpha+\tau_\gamma+6}{2}\right)_3(2a)^{1/2}(d_\alpha g_\gamma+g_\alpha+d_\gamma)U_{\tau_\alpha+\tau_\gamma+12}$$
$$\left.+\left(\frac{\tau_\alpha+\tau_\gamma+6}{2}\right)_4 g_\alpha g_\gamma U_{\tau_\alpha+\tau_\gamma+14}\right]. \tag{A.5}$$

Here one has to select the integrals that are necessary to calculate transitions with $\Delta\tau = \pm 1$. The remaining transitions must be forbidden in the τ degree of freedom, if the O(5) symmetry is correct.

For the matrix elements of the E0 operator the $\delta = 2$ choice has to be made in (A.3):

$$W^2_{\alpha,\gamma} = N_\alpha N_\gamma \frac{1}{2}\Gamma\left(\frac{\tau_\alpha+\tau_\gamma+7}{2}\right)(2a)^{-(\tau_\alpha+\tau_\gamma+15)/4}$$
$$\times\left[(2a)^2U_{\tau_\alpha+\tau_\gamma+7}+\frac{\tau_\alpha+\tau_\gamma+7}{2}(2a)^{3/2}(d_\alpha+d_\gamma)U_{\tau_\alpha+\tau_\gamma+9}\right.$$
$$+\left(\frac{\tau_\alpha+\tau_\gamma+7}{2}\right)_2(2a)(d_\alpha d_\gamma+g_\alpha+g_\gamma)U_{\tau_\alpha+\tau_\gamma+11}$$
$$+\left(\frac{\tau_\alpha+\tau_\gamma+7}{2}\right)_3(2a)^{1/2}(d_\alpha g_\gamma+g_\alpha d_\gamma)U_{\tau_\alpha+\tau_\gamma+13}$$
$$\left.+\left(\frac{\tau_\alpha+\tau_\gamma+7}{2}\right)_4 g_\alpha g_\gamma U_{\tau_\alpha+\tau_\gamma+15}\right]. \tag{A.6}$$

In this case we calculate only $0^+ \to 0^+$ transitions, so we have only a few integrals.

ORCID iDs

G Lévai https://orcid.org/0000-0003-3785-3165
J M Arias https://orcid.org/0000-0001-7363-4328

References

[1] Bohr A and Mottelson B 1975 *Nuclear Structure* vol 2 (New York: Benjamin)
[2] Iachello F and Arima A 1987 *The Interacting Boson Mode* (Cambridge: Cambridge University Press)
[3] Ginocchio J N and Kirson M W 1980 *Phys. Rev. Lett.* **44** 1744
[4] Ginocchio J N and Kirson M W 1980 *Nucl. Phys.* A **350** 31
[5] Iachello F 2000 *Phys. Rev. Lett.* **85** 3580
[6] Casten R F 2006 *Nat. Phys.* **2** 811
[7] Casten R F and McCutchan E A 2007 *J. Phys. G: Nucl. Part. Phys.* **34** R285
[8] Bonatsos D, Lenis D and Petrellis D 2007 *Rom. Rep. Phys.* **59** 273
[9] Casten R F 2009 *Prog. Part. Nucl. Phys.* **62** 183
[10] Cejnar P and Jolie J 2009 *Prog. Part. Nucl. Phys.* **62** 210
[11] Cejnar P, Jolie J and Casten R F 2010 *Rev. Mod. Phys.* **82** 2155
[12] Rowe D J, Welsh T A and Caprio M A 2008 *Phys. Rev.* C **79** 054304
[13] Caprio M A 2011 *Phys. Rev.* C **83** 064309
[14] Turbiner A V 2016 *Phys. Rep.* **642** 1
[15] Ushveridze A G 1994 *Quasi-exactly Solvable Models in Quantum Mechanics* (Bristol: Institute of Physics Publishing)
[16] Lévai G and Arias J M 2004 *Phys. Rev.* C **69** 014304
[17] Lévai G and Arias J M 2010 *Phys. Rev.* C **81** 044304
[18] Raduta A A and Buganu P 2011 *Phys. Rev.* C **83** 034313
[19] Raduta A A and Buganu P 2013 *J. Phys. G: Nucl. Part. Phys.* **40** 025108
[20] Buganu P and Budaca R 2015 *Phys. Rev.* C **91** 014306
[21] Buganu P and Budaca R 2015 *J. Phys. G: Nucl. Part. Phys.* **42** 105106
[22] Budaca R, Buganu P, Chabab M, Lahbas A and Oulne M 2016 *Ann. Phys., NY* **375** 65
[23] Budaca R, Budaca A I and Buganu P 2019 *J. Phys. G: Nucl. Part. Phys.* **46** 125101
[24] Lahbas A, Buganu P and Budaca R 2020 *Mod. Phys. Lett.* A **35** 2050085
[25] Bès D R 1959 *Nucl. Phys.* **10** 373
[26] Yannouleas C and Pacheco J M 1989 *Comput. Phys. Commun.* **54** 315
[27] Rowe D J, Turner P S and Repka J 2004 *J. Math. Phys.* **45** 2761
[28] Moshinsky M and Smirnov Y 1996 *The Harmonic Oscillator in Modern Physics* (Amsterdam: Harwood Academic Publishers)
[29] Wilets L and Jean M 1956 *Phys. Rev.* **102** 788
[30] Garrett P E *et al* 2019 *Phys. Rev. Lett.* **123** 142502
[31] Leviatan A, Gavrielov N, García-Ramos J E and Van Isacker P 2018 *Phys. Rev.* C **98** 031302(R)
[32] National Nuclear Data Center https://nndc.bnl.gov/ensdf/DatasetFetchServlet
[33] Budaca R and Buganu P 2019 *Phys. Rev.* C **100** 049801
[34] Caprio M A and Iachello F 2007 *Nucl. Phys.* A **781** 26
[35] Arias J M 2001 *Phys. Rev.* C **63** 034308
[36] Abramowitz M and Stegun I A 1970 *Handbook of Mathematical Functions* (New York: Dover)
[37] Casten R F and Cakirli R B 2016 *Phys. Scr.* **91** 033004
[38] Dobaczewski J, Nazarewicz W and Reinhard P-G 2014 *J. Phys. G: Nucl. Part. Phys.* **41** 074001